# The Oxygen Isotopic Composition of Samples Returned from Asteroid Ryugu with Implications for the Nature of the Parent Planetesimal

Haolan Tang[1,2], Edward D. Young[1], Lauren Tafla[1], Andreas Pack[3], Tommaso Di Rocco[3], Yoshinari Abe[4], Jérôme Aléon[5], Conel M. O'D. Alexander[6], Sachiko Amari[7], Yuri Amelin[8], Ken-ichi Bajo[9], Martin Bizzarro[10], Audrey Bouvier[11], Richard W. Carlson[6], Marc Chaussidon[12], Byeon-Gak Choi[13], Nicolas Dauphas[14], Andrew M. Davis[14], Wataru Fujiya[15], Ryota Fukai[16], Ikshu Gautam[17], Makiko K. Haba[17], Yuki Hibiya[18], Hiroshi Hidaka[19], Hisashi Homma[20], Peter Hoppe[21], Gary R. Huss[22], Kiyohiro Ichida[23], Tsuyoshi Iizuka[24], Trevor R. Ireland[25], Akira Ishikawa[26], Motoo Ito[26], Shoichi Itoh[27], Noriyuki Kawasaki[9], Noriko T. Kita[28], Kouki Kitajima[28], Thorsten Kleine[29], Shintaro Komatani[23], Alexander N. Krot[22], Ming-Chang Liu[30], Yuki Masuda[17], Kevin D. McKeegan[1], Mayu Morita[23], Kazuko Motomura[31], Frédéric Moynier[12], Kazuhide Nagashima[22], Izumi Nakai[32], Ann Nguyen[33], Larry Nittler[34], Morihiko Onose[23], Changkun Park[35], Laurette Piani[36], Liping Qin[2], Sara S. Russell[37], Naoya Sakamoto[38], Maria Schönbächler[39], Kentaro Terada[40], Yasuko Terada[41], Tomohiro Usui[15], Sohei Wada[9], Meenakshi Wadhwa[42], Richard J. Walker[43], Katsuyuki Yamashita[44], Qing-Zhu Yin[45], Tetsuya Yokoyama[17], Shigekazu Yoneda[46], Hiroharu Yui[47], Ai-Cheng Zhang[48], Tomoki Nakamura[49], Hiroshi Naraoka[50], Takaaki Noguchi[27], Ryuji Okazaki[50], Kanako Sakamoto[16], Hikaru Yabuta[51], Masanao Abe[16], Akiko Miyazaki[16], Aiko Nakato[16], Masahiro Nishimura[16], Tatsuaki Okada[16], Toru Yada[16], Kasumi Yogata[16], Satoru Nakazawa[16], Takanao Saiki[16], Satoshi Tanaka[16], Fuyuto Terui[52], Yuichi Tsuda[16], Sei-ichiro Watanabe[19], Makoto Yoshikawa[16], Shogo Tachibana[53], and Hisayoshi Yurimoto[19,38]

[1] Earth, Planetary, and Space Sciences, UCLA, Los Angeles, CA 90095, USA; haolantang@ustc.edu.cn, eyoung@epss.ucla.edu
[2] School of Earth and Space Sciences, University of Science and Technology of China, Anhui, 230026, University of Science and Technology of China, People's Republic of China
[3] Abteilung Isotopogengeologie, Universitat Göttingen, Göttingen D-37077, Germany
[4] Graduate School of Engineering Materials Science and Engineering, Tokyo Denki University, Tokyo 120-8551, Japan
[5] Institut de Minéralogie, de Physique des Matériaux et de Cosmochimie, Sorbonne Université, Museum National d'Histoire Naturelle, CNRS UMR 7590, IRD, Paris 75005, France
[6] Earth and Planets Laboratory, Carnegie Institution for Science, 5241 Branch Road NW, Washington, DC 20015 USA
[7] McDonnell Center for the Space Sciences and Physics Department, Washington University, St. Louis, MO 63130, USA
[8] Guangzhou Institute of Geochemistry, Chinese Academy of Sciences, Guangzhou, GD 510640, People's Republic of China
[9] Department of Natural History Sciences, Hokkaido University, Sapporo 001-0021, Japan
[10] Centre for Star and Planet Formation, GLOBE Institute, University of Copenhagen, Copenhagen K 1350, Denmark
[11] Bayerisches Geoinstitut, Universität Bayreuth, Bayreuth 95447, Germany
[12] Université de Paris, Institut de physique du globe de Paris, CNRS Paris 75005, France
[13] Department of Physics and Astronomy, Seoul National University, Seoul 08826, Republic of Korea
[14] Department of the Geophysical Sciences and Enrico Fermi Institute, The University of Chicago, 5734 South Ellis Avenue, Chicago, IL 60637, USA
[15] Faculty of Science, Ibaraki University, Mito 310-8512, Japan
[16] Institute of Space and Astronautical Science, Japan Aerospace Exploration Agency, Sagamihara 252-5210, Japan
[17] Department of Earth and Planetary Sciences, Tokyo Institute of Technology, Tokyo 152-8551, Japan
[18] General Systems Studies, The University of Tokyo, Tokyo 153-0041, Japan
[19] Earth and Planetary Sciences, Nagoya University, Nagoya 464-8601, Japan
[20] Osaka Application Laboratory, SBUWDX, Rigaku Corporation, Osaka 569-1146, Japan
[21] Max Planck Institute for Chemistry, Mainz 55128, Mainz 55128, Germany
[22] Hawai'i Institute of Geophysics and Planetology, University of Hawai'i at Mānoa, Honolulu, HI 96822, USA
[23] Analytical Technology, Horiba Techno Service Co., Ltd., Kyoto 601-8125, Japan
[24] Earth and Planetary Science, The University of Tokyo, Tokyo 113-0033, Japan
[25] School of Earth and Environmental Sciences, The University of Queensland, St. Lucia, QLD 4072, Australia
[26] Kochi Institute for Core Sample Research, JAMSTEC, Kochi 783-8502, Japan
[27] Division of Earth and Planetary Sciences, Kyoto University, Kyoto 606-8502, Japan
[28] Department of Geoscience, University of Wisconsin−Madison, Madison, WI 53706, USA
[29] Max Planck Institute for Solar System Research, Göttingen 37077, Germany
[30] Lawrence Livermore National Laboratory, CA 94550, USA
[31] Thermal Analysis, Rigaku Corporation, Tokyo 196-8666, Japan
[32] Applied Chemistry, Tokyo University of Science, Tokyo 162-8601, Japan
[33] Astromaterials Research and Exploration Science, NASA Johnson Space Center, Houston, TX 77058, USA
[34] School of Earth and Space Exploration, Arizona State University, Tempe, AZ 85281, USA
[35] Earth-System Sciences, Korea Polar Research Institute, Incheon 21990, Republic of Korea
[36] Centre de Recherches Pétrographiques et Géochimiques, CNRS—Université de Lorraine, Nancy 54500, France
[37] Department of Earth Sciences, Natural History Museum, London SW7 5BD, UK
[38] Isotope Imaging Laboratory, Creative Research Institution, Hokkaido University, Sapporo 001-0021, Japan
[39] Institute for Geochemistry and Petrology, Department of Earth Sciences, ETH Zurich, Switzerland
[40] Earth and Space Science, Osaka University, Osaka 560-0043, Japan
[41] Spectroscopy and Imaging, Japan Synchrotron Radiation Research Institute, Hyogo 679-5198, Japan
[42] School of Earth and Space Exploration, Arizona State University, Tempe, AZ 85281, USA
[43] Department of Geology, University of Maryland, College Park, MD 20742, USA
[44] Graduate School of Natural Science and Technology, Okayama University, Okayama 700-8530, Japan
[45] Department of Earth and Planetary Sciences, University of California, Davis, Davis, CA 95616, USA
[46] Department of Science and Engineering, National Museum of Nature and Science, Tsukuba 305-0005, Japan
[47] Department of Chemistry, Tokyo University of Science, Tokyo 162-8601, Japan
[48] School of Earth Sciences and Engineering, Nanjing University, Nanjing 210023, Nanjing 210023, People's Republic of China
[49] Department of Earth Science, Tohoku University, Sendai 980-8578, Japan

[50] Department of Earth and Planetary Sciences, Kyushu University, Fukuoka 819-0395, Japan
[51] Earth and Planetary Systems Science Program, Hiroshima University, Higashi-Hiroshima 739-8526, Japan
[52] Kanagawa Institute of Technology, Atsugi 243-0292, Japan
[53] UTokyo Organization for Planetary and Space Science, University of Tokyo, Tokyo 113-0033, Japan

## Abstract

We present oxygen isotopic analyses of fragments of the near-Earth $C_b$-type asteroid Ryugu returned by the Hayabusa2 spacecraft that reinforce the close correspondence between Ryugu and CI chondrites. Small differences between Ryugu samples and CI chondrites in $\Delta'^{17}O$ can be explained at least in part by contamination of the latter by terrestrial water. The discovery that a randomly sampled C-complex asteroid is composed of CI-chondrite-like rock, combined with thermal models for formation prior to significant decay of the short-lived radioisotope $^{26}Al$, suggests that if lithified at the time of alteration, the parent body was small ($\ll$50 km radius). If the parent planetesimal was large ($>$50 km in radius), it was likely composed of high-permeability, poorly lithified sediment rather than consolidated rock.

*Unified Astronomy Thesaurus concepts:* Asteroids (72); Planetary thermal histories (2290); Carbonaceous chondrites (200)

## 1. Introduction

The JAXA Hayabusa2 spacecraft was launched on 2014 December 3 with the goal of returning samples from the near-Earth $C_b$-type asteroid (162173) Ryugu (Tachibana et al. 2014, 2022). Two samples were obtained from two separate touchdown sites on Ryugu in 2019, and the collected samples were delivered to Earth on 2020 December 6 (Morota et al. 2020). Analysis by the Initial Analysis Chemistry Team reveals that the Ryugu samples have clear mineralogical and chemical affinities to CI (Ivuna group) chondrite meteorites (Yokoyama et al. 2023).

Despite their rarity among meteorite samples, CI chondrites play a unique role in our understanding of the formation of the solar system because in most cases their elemental compositions are indistinguishable from those of rock-forming elements comprising the solar photosphere, excluding some volatile elements (Lodders 2021). However, the ubiquity of secondary minerals such as carbonates and phyllosilicates in CI chondrites (e.g., Tomeoka & Buseck 1988; Brearley 2006) indicates pervasive water–rock interactions in these rocks, which belies their primitive chemical nature. A persistent question has been whether these highly altered rocks are rare, as their frequency among meteorites would suggest, or rather whether they are common among the vestiges of planetesimals in our solar system. With the discovery that at least one near-Earth asteroid is composed of CI chondrite-like rocks, with extensive aqueous alteration, the prospect that reactions between water and rocks were common in primitive plantesimals is enhanced.

Both CI chondrites and the Ryugu samples exhibit similar degrees of aqueous alteration in which the rocks are almost entirely converted to phyllosilicates, carbonates, magnetite, and secondary sulfides. One difference between CI chondrites and the Ryugu samples is the lack of significant interlayer water in the expandable clay minerals comprising Ryugu samples relative to CI meteorites (Wasson & Kallemeyn 1988; Yokoyama et al. 2023). The cause of this disparity in interlayer water content is the subject of much speculation and may include some combination of contamination of the meteorite clay minerals by terrestrial water and loss of interlayer water from Ryugu samples to the vacuum of space.

In this paper, we present the bulk oxygen isotopic measurements of the Ryugu samples A0107 and C0002 from the two distinct touchdown sites. Heating experiments were also performed to dehydrate CI chondrites with the aim of exploring the impact of interlayer water on bulk oxygen isotopic compositions. We use these results to quantify the link between rocks from Ryugu and CI chondrite meteorites, and we draw conclusions about the nature of the planetesimals represented by these samples.

## 2. Materials and Methods

### 2.1. Methods at UCLA

#### 2.1.1. Fluorination and Mass Spectrometry

Two aliquots with masses of 1.50 mg (sample B) and 2.58 mg (sample C) from A0107 were analyzed. For comparison, three Orgueil samples (3.06, 4.27, and 4.31 mg) and three Orgueil samples experiencing heating experiments ($\sim$5 mg before heating) were analyzed using the same methods. Heating experiments were performed in a GSL-1000X-S furnace accessing a pump station to maintain vacuum ($\sim$1.6 $\times$ $10^{-6}$ mbar). The Orgueil samples were loaded into the furnace using a 2 ml quartz boat. The masses were weighed before and after heating experiments to estimate mass losses associated with different experimental conditions.

A stainless steel sample holder with Ryugu aliquots and Orgueil samples was loaded into the chamber for analyses with a baseline pressure of $\sim$5 $\times$ $10^{-7}$ mbar. To eliminate surface absorbing water, samples were then heated with an infrared lamp while actively pumping for approximately 2–3 hr. The temperature of the samples inside the chamber during heating can reach $\sim$110°C–120°C as deduced by thermal imaging of analogous CI meteorite samples through the ZnSe window of the chamber under identical conditions (Figure A1).

$O_2$ from the samples was extracted by using a laser-heating-assisted fluorination system. Around 90 mbar of double-distilled $F_2$ was loaded into the sample chamber as the fluorinating agent (Young et al. 1998). The heating laser is a 20 W $CO_2$ laser (10.6 $\mu$m) gated with a pulse frequency of 10 Hz (Sharp 1990). Completing fluorination for each sample takes about 10–15 minutes. The product gas was then purified in the vacuum system by passing through a KBr trap warmed to 110°C with cold traps located at both sides (cooled with liquid $N_2$). In this stage, $SiF_4$ and the remaining $F_2$ were trapped by KBr, and the product $Br_2$ was condensed into the cold traps.

The extracted $O_2$ was then collected into a 13X molecular sieve cooled by liquid $N_2$ for 60 minutes. This trap was then heated up to 210°C to expand the purified $O_2$ for yield calculation. The $O_2$ then was collected into a sample vial filled with silica gel at liquid $N_2$ temperature for isotopic measurement on the mass spectrometer.

Isotope ratios were determined by measuring $^{32}O_2^+$, $^{33}O_2^+$, and $^{34}O_2^+$ on a high mass resolution, double-focusing gas-source mass spectrometer at UCLA (Nu Instruments Panorama 001). The mass resolving power ($M/\Delta M$) of 40,000 used for these measurements is sufficient to resolve mass interferences, the most important of which is trace $NF^+$ that is a potential mass spectrometric isobar for $^{33}O_2^+$ (i.e., $^{17}O^{16}O^+ + {}^{16}O^{17}O^+$; Young et al. 2016). The $^{32}O_2^+$, $^{33}O_2^+$, and $^{34}O_2^+$ ion beams were measured using Faraday cups with amplifier resistors of $10^{10}\Omega$, $10^{13}\Omega$, and $10^{11}\Omega$, respectively. Analyses were achieved from three and six blocks for samples B and C, respectively. Each block comprised 30 cycles of sample/reference gas comparisons, and each cycle took 30 s for signal integration.

The reference gas was calibrated using $O_2$ purified by gas chromatography from air ($\delta^{18}O = -11.524$‰, $\delta^{17}O = -6.099$‰). To guarantee the accuracy of the measurements, San Carlos olivines (SC olivine), a common geostandard for rock and mineral oxygen isotope analyses, were also analyzed in the same analytical sessions for the two Ryugu samples at UCLA, yielding $\Delta^{17}O = -0.065 \pm 0.005$‰ ($\Delta^{17}O = \delta^{17}O_{VSMOW} - 0.52 \times \delta^{18}O_{VSMOW}$) by average. Our results for SC olivine are consistent with the recent study that SC olivine has a $\Delta^{17}O$ of $\sim -0.05$ to $-0.1$‰ relative to the standard mean ocean water (SMOW; Pack 2021), implying that bulk silicate Earth (BSE) also has a $\Delta^{17}O$ lower than SMOW by as much as $\sim -0.1$‰. Two analyses of air during this interval yielded $\Delta^{17}O = -0.265 \pm 0.032$‰ by average.

### 2.1.2. $\Delta^{17}O$ versus $\Delta'^{17}O$

For purposes of comparisons with previous work, we utilize the logarithmic definitions of fractional deviations from standards represented by the delta notation (Young et al. 2002), in which $\delta'^i O_{SMOW} = 10^3 \ln(^i R_{sample}/^i R_{SMOW})$; $^i R$ denotes the indicated oxygen isotope ratio $^i O/^{16}O$, where $i = 17$ or $18$; and $\Delta'^{17}O = \delta'^{17}O_{SMOW} - \beta \times \delta'^{18}O_{SMOW}$. Here mass-dependent fractionation is well represented by $\beta = 0.528$ (Miller 2002; Young et al. 2002; Rumble et al. 2007; Tanaka & Nakamura 2013; Pack & Herwartz 2014; Young et al. 2014, 2016). With these definitions, our SC olivine analyses obtained during the Ryugu analytical session give $\Delta'^{17}O = -0.104 \pm 0.006$‰, and the value for air is $-0.380 \pm 0.031$‰. Both values are consistent with the previous work. The two A0107 Ryugu samples B and C have $\Delta'^{17}O$ values of $0.576 \pm 0.056$‰ and $0.574 \pm 0.019$‰ using this prime notation that more accurately reflects mass fractionation.

Note that for the same samples the values of $\Delta'^{17}O$ are lower than $\Delta^{17}O$ calculated using $\delta^{18}O_{SMOW}$ and $\delta^{17}O_{SMOW}$ (fractional differences, not logs of ratios), where $\delta^i O_{SMOW} = 10^3(^i R_{sample}/^i R_{SMOW} - 1)$ and $i = 17$ or $18$, by up to $0.1$‰. For instance, for a sample with $\delta^{18}O_{SMOW}$ of $15$‰ and $\delta^{17}O_{SMOW}$ of $8.45$‰, $\Delta^{17}O = 0.65$‰ using the strictly linear mass fractionation law in which $\delta^{17}O = 0.52 \times \delta^{18}O$. However, with the corresponding $\delta'^{18}O_{SMOW}$ and $\delta'^{17}O_{SMOW}$ values of $14.89$‰ and $8.41$‰, respectively, $\Delta'^{17}O = 0.55$‰ with $\beta = 0.528$. Thus, comparison of the results of Ryugu samples

among different laboratories must be made based on consistent $\delta$ notation. For the case of bulk oxygen isotopic analyses of Ryugu samples, the $\Delta'^{17}O$ values from A0107 obtained at UCLA are $0.576 \pm 0.056$‰ and $0.574 \pm 0.019$‰, and the $\Delta'^{17}O$ values from C0009 obtained at University of Göttingen are $0.37 \pm 0.056$‰ and $0.374 \pm 0.019$‰. On the other hand, seven aliquots from Ryugu samples including Chamber A and Chamber C were analyzed at Open University, giving an average $\Delta^{17}O = 0.65 \pm 0.10$‰ and $\delta^{18}O_{SMOW} = \sim 15$‰ (Greenwood et al. 2023). Recasting their results into the logarithmic delta notation results in $\Delta'^{17}O$ of $0.55$, identical to the $\Delta'^{17}O$ values obtained at UCLA.

### 2.1.3. Raman Spectroscopy

Heating experiments were performed on two Orgueil fragments. One was heated at 120°C for 2 hr, and the other one was heated at 350°C for 5 hr. After heating experiments, both fragments were mounted in epoxy. In addition, an unheated Orgueil fragment was also mounted for comparison. The mounts were polished using SiC abrasive paper down to 3 $\mu$m without any fluid in order to prohibit water contamination. The sample surfaces were cleaned by air flow and scotch tape frequently during sample preparation. We obtained the Raman spectra of the spot samples by a Horiba LabRam HR Evolution Raman spectrometer. The system has a BXFM microscope and a Synapse charge-coupled device (CCD) detection system, motorized XYZ stage, VIS camera, and five microscope objectives with magnifications up to 50. The system is controlled through LabSpec 6.4.2.5 software. The Oxxius laser at 532 nm (maximum power 100 mW) was used for excitation. The Raman spectrometer has a point-and-shoot Raman capability of $\sim 5$ $\mu$m spatial resolution. We used the $50\times$ objective together with the laser source at 532 nm with power at 50%. The Raman spectra were collected from 2500 to 4000 $cm^{-1}$ with a spectral resolution of $0.37$ $cm^{-1}$ and an accumulation time of 5–10 s. A silica chip was used for wavelength calibration.

The spectra presented in the text represent the average spectra signals of 9–13 spots for each sample. The local baselines were fit with linear functions. The region of Raman spectra corresponding to water stretching modes, from 3000 to 3800 $cm^{-1}$ (e.g., Shahar & Bassett 2005; Kolesov 2006; de Ligny et al. 2013; Grishina et al. 2021), was fit using Lorentzian line shapes (Bancroft et al. 2018). Five bands of molecular water at 3066, 3194, 3306, 3400, and 3510 $cm^{-1}$ were used to fit the spectra. The areas relative to the area of the band for C–H bonds at 2800–3000 $cm^{-1}$ (Bulkin & Krishnan 1971; Romero-Pastor et al. 2011) are consistent from sample to sample, permitting the C–H bands to be used to normalize the spectra to one another.

### 2.2. Methods at UG

Two aliquots (1.42 and 1.30 mg) from Ryugu sample C0002 were analyzed. For comparison, two aliquots of the Orgueil CI chondrite (1.21 and 1.14 mg) and an aliquot of the Ivuna CI chondrite (0.92 mg) were analyzed using the same methods. The details were described previously by Yokoyama et al. (2023). To avoid any contamination, analyses were conducted using small, two-pit sample holders loaded from an evacuated air lock into the chamber. The air lock was pumped down to $\sim 5 \times 10^{-6}$ mbar and heated up to 100°C for 24 hr using

**Table 1**
Summary of Oxygen Isotope Data for Ryugu and Chondrites

| Samples | | $\delta^{18}O$ (1$\sigma$) | $\delta^{17}O$ (1$\sigma$) | $\Delta^{17}O$ (1$\sigma$) | $\Delta'^{17}O$ (1$\sigma$) |
|---|---|---|---|---|---|
| *UCLA* | | | | | |
| *Ryugu A0107* | | | | | |
| Sample B | | 20.059 ± 0.024 | 11.123 ± 0.055 | 0.694 ± 0.056 | 0.576 ± 0.056 |
| Sample C | | 17.293 ± 0.012 | 9.673 ± 0.018 | 0.681 ± 0.019 | 0.574 ± 0.019 |
| *CI chondrites* | | | | | |
| Orgueil | | 17.474 ± 0.008 | 9.598 ± 0.014 | 0.512 ± 0.015 | 0.405 ± 0.015 |
| | | 19.056 ± 0.006 | 10.438 ± 0.011 | 0.529 ± 0.011 | 0.416 ± 0.011 |
| | | 14.721 ± 0.005 | 8.078 ± 0.010 | 0.423 ± 0.010 | 0.330 ± 0.010 |
| | | 17.166 ± 0.007 | 9.322 ± 0.011 | 0.396 ± 0.012 | 0.292 ± 0.012 |
| *CV chondrites* | | | | | |
| Allende | | 1.218 ± 0.038 | −2.881 ± 0.062 | −3.514 ± 0.065 | −3.527 ± 0.065 |
| | | 5.255 ± 0.007 | 0.253 ± 0.013 | −2.480 ± 0.014 | −2.509 ± 0.013 |
| | | 4.427 ± 0.008 | −0.296 ± 0.018 | −2.598 ± 0.018 | −2.628 ± 0.018 |
| *Heating experiments (heating time: 5 hr)* | mass loss | | | | |
| Orgueil (250°C) | 7.5% | 20.129 ± 0.006 | 10.913 ± 0.010 | 0.446 ± 0.011 | 0.331 ± 0.010 |
| Orgueil (350°C) | 13.9% | 22.606 ± 0.006 | 12.238 ± 0.010 | 0.483 ± 0.011 | 0.360 ± 0.010 |
| | 24.1% | 24.137 ± 0.006 | 13.130 ± 0.011 | 0.579 ± 0.011 | 0.452 ± 0.011 |
| *University of Göttingen* | | | | | |
| *Ryugu C0002* | | | | | |
| Aliquot1 | | 19.82 ± 0.15 | 10.72 ± 0.08 | 0.41 ± 0.01 | 0.30 ± 0.01 |
| Aliquot 2 | | 19.74 ± 0.15 | 10.69 ± 0.08 | 0.43 ± 0.018 | 0.31 ± 0.01 |
| *CI chondrites* | | | | | |
| Orgueil | | 13.44 ± 0.15 | 7.56 ± 0.08 | 0.57 ± 0.01 | 0.47 ± 0.01 |
| | | 13.61 ± 0.15 | 7.64 ± 0.08 | 0.56 ± 0.01 | 0.47 ± 0.01 |
| | | 13.59 ± 0.15 | 7.61 ± 0.08 | 0.54 ± 0.01 | 0.46 ± 0.01 |
| | | 13.47 ± 0.15 | 7.57 ± 0.08 | 0.56 ± 0.01 | 0.48 ± 0.01 |
| | | 13.94 ± 0.15 | 7.64 ± 0.08 | 0.39 ± 0.01 | 0.30 ± 0.01 |
| Alais | | 14.07 ± 0.15 | 8.19 ± 0.08 | 0.87 ± 0.01 | 0.78 ± 0.01 |
| Ivuna | | 13.96 ± 0.15 | 7.67 ± 0.08 | 0.87 ± 0.01 | 0.32 ± 0.01 |
| *CM chondrites* | | | | | |
| Murchison | | 5.16 ± 0.15 | −0.52 ± 0.08 | −3.20 ± 0.01 | −3.24 ± 0.01 |

heating tape. The empty fluorination chamber was heated to about 60°C for 24 hr before loading ∼50–100 mbar BrF$_5$ for ∼15 minutes to eliminate any moisture in the chamber. The O$_2$ blank was monitored by means of continuous flow mass spectrometry until it stabilized after roughly seven fluorination steps at 0.01–0.02 $\mu$mol O$_2$.

Sample holders (∼5 × 10 × 8 mm$^3$) were introduced into the fluorination chamber through a gate valve. Samples were exposed to BrF$_5$ (100–300 mbar) for ∼10 minutes prior to laser heating. Fluorination of the sample was undertaken while increasing the laser power up to a maximum of 45 W.

After fluorination, the liberated O$_2$ gas was transferred via cold traps and an NaCl getter to a 5 Å molecular sieve trap. F$_2$ was removed in the NaCl getter. Then, O$_2$ was transferred by He gas flow through a gas chromatography column (GC, 3 m, 1/8″, 50°C) into the second molecular sieve trap connected to the Thermo 253 Plus mass spectrometer dual inlet. O$_2$ was expanded into a sample bellows on the mass spectrometer after evacuating He from the system.
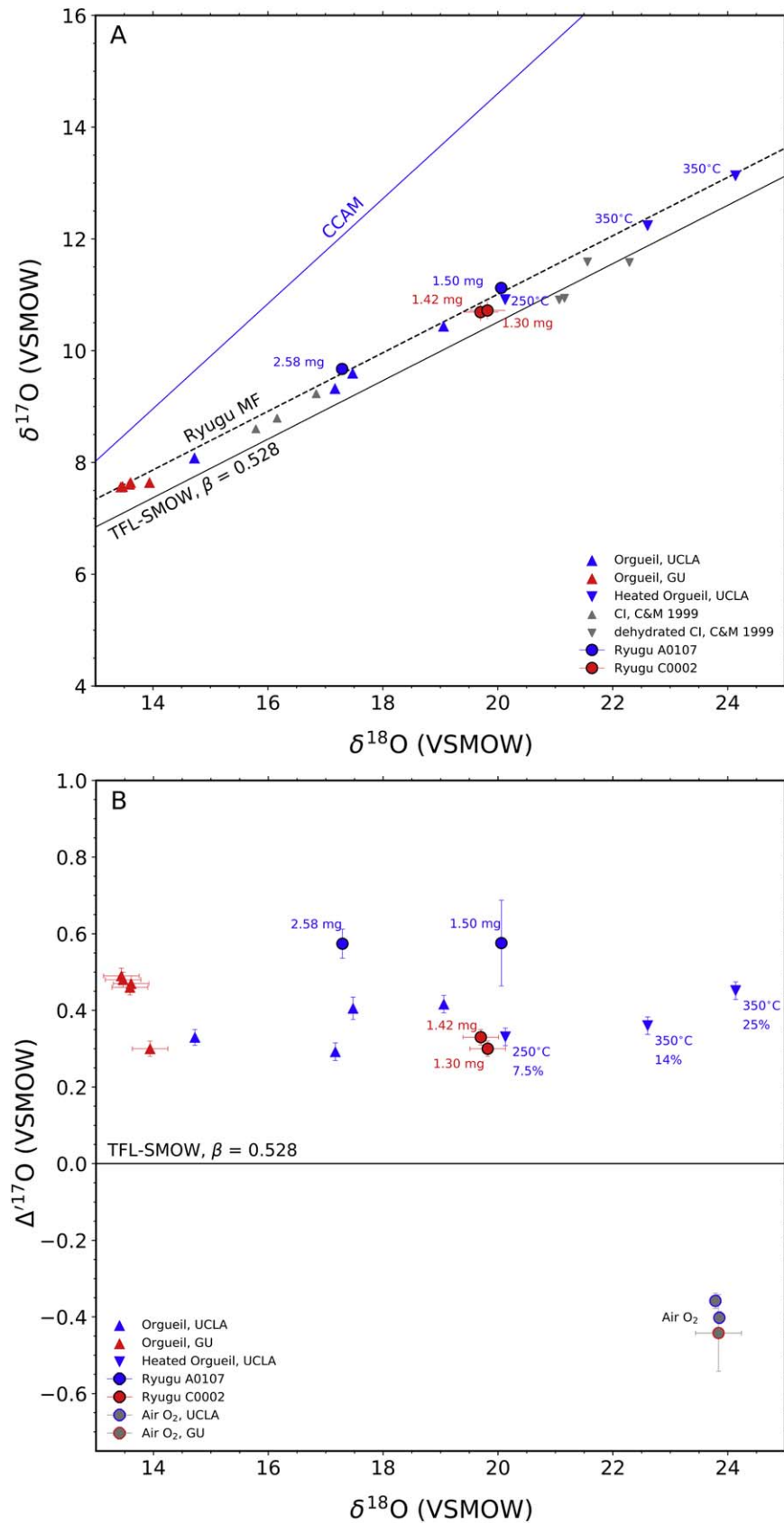
## 3. Results

Table 1 and Figure 1 exhibit $\delta'^{17}O$, $\delta'^{18}O$, and $\Delta'^{17}O$ of Ryugu samples, as well as carbonaceous chondrites. Despite the differences in methods, the two laboratories obtain similar results for terrestrial standards (see Table A1 in Appendix A). The two aliquots from Chamber A (A0107) of Ryugu measured

at UCLA, with masses of 2.58 and 1.50 mg, have $\delta^{18}O$ values of 17.293‰ ± 0.012‰ and 20.059‰ ± 0.024‰ (1$\sigma$), respectively. These values are slightly higher than the average of Orgueil obtained at UCLA ($\delta^{18}O$ = 17.104‰ ± 0.896‰, $n$ = 4). Despite the distinct $\delta^{18}O$, $\Delta'^{17}O$ in both samples are identical to each other, yielding an average of 0.575‰ ± 0.003‰ (Figure 1(b)). This value is higher by 0.1‰ compared to the maximum value for Orgueil from both UCLA and Göttingen and from the literature (Clayton & Mayeda 1999). The Ryugu sample from Chamber C (C0002), with masses of 1.42 and 1.30 mg, was analyzed at Göttingen. The average $\delta^{18}O$ and $\Delta'^{17}O$ are 19.8‰ and 0.30‰ ± 0.002‰, respectively. As shown in Figure 1(b), the $\delta^{18}O$ of Ryugu samples is significantly higher by ∼5‰ compared to those of Orgueil measured at Göttingen.

Heating experiments on Orgueil powders were achieved in a GSL-1000X-S furnace connected to Pfeiffer HiCUBE pump station in order to conduct the heating experiment in vacuum. Four heating conditions were set with the aim to remove different forms of water from Orgueil. As shown in Figure 1 and Table 1, our results over 5 hr exhibit mass losses of 7.5%, 13.9%, and 24.9%, corresponding to the $\Delta'^{17}O$ of 0.331‰ ± 0.010‰, 0.360‰ ± 0.010‰, and 0.452‰ ± 0.011‰, respectively. Likewise, dehydration under the vacuum significantly shifts $\delta^{18}O$ up to 23.85‰ ± 0.01‰, and the degree of this shift is also associated with the mass loss of heated samples.

**Figure 1.** (a) Oxygen three-isotope plot comparing Ryugu milligram-sized samples (circles) with Orgueil meteorite values from this study and from the literature (triangles). (b) Plot of $\Delta'^{17}O$ vs. $\delta^{18}O$ showing the results of Ryugu samples together with Orgueil meteorites (unheated vs. heated; heating temperature and mass-loss fraction are labeled in blue) and geostandards. "Ryugu MF" denotes the Ryugu mass-dependent fractionation curve (black dashed line) with $\beta = 0.528$; C&M refers to Clayton & Mayeda (1999).

## 4. Discussion

### 4.1. $\Delta'^{17}O$ in Ryugu Samples Relative to CI Chondrites: Sample Heterogeneity or Influence of Terrestrial Water?

The differences between oxygen isotope analyses from the two laboratories are greater than the differences in standards between the laboratories, suggesting that whole-rock $\Delta'^{17}O$ is variable on the order of 0.1‰ at the milligram scale among Ryugu samples. Larger variations among oxide and carbonate minerals, anomalous silicates, and tiny grains of olivine and pyroxene also present in relatively small mass fractions may also contribute to this variability in bulk $\Delta'^{17}O$ values (Liu et al. 2022; McCain et al. 2023; Nakashima et al. 2023). The $\delta^{18}O$ values of these samples vary over several per mil, presumably for similar reasons. Ryugu samples are mixtures of brecciated fine-grained matrix materials composed of predominantly phyllosilicates (serpentine and saponite) and coarser grains dominated by carbonates, magnetite, and sulfide (Yokoyama et al. 2023). In situ analyses of oxygen isotopic compositions of magnetite have $\Delta'^{17}O$ that vary from about 0‰ to about 3‰, and carbonates exhibit a range in $\Delta'^{17}O$ values of ±1‰ (Liu et al. 2022; McCain et al. 2023; Nakashima et al. 2023). Due to such diverse oxygen isotopic ratios in different minerals, one expects that heterogeneous mineral distributions can result in variable oxygen isotopic compositions among millimeter-size Ryugu samples. A similar scale of dispersion in oxygen isotopic ratios is also observed in the bulk Orgueil analyses from this study and in literature data (Clayton & Mayeda 1999). Thus, the distinct $\Delta'^{17}O$ values in Ryugu samples obtained from the two laboratories can be explained in part as the result of variable modal abundances of constituent minerals among different particles of Ryugu (Dauphas & Pourmand 2015).

Another explanation for small differences between oxygen isotopic ratios in Ryugu samples and those from CI chondrites could be their disparate interlayer water contents (Vacher et al. 2020). Mass-loss differential thermogravimetric (DTG) and released-molecule curves for Ryugu samples compared to CI chondrites suggest that the Ryugu samples are significantly depleted in interlayer water (Yokoyama et al. 2023) despite having saponite as a significant constituent. The discrepancy in $\Delta'^{17}O$ in Ryugu samples relative to many CI chondrites therefore could be attributed to the depletion of interlayer water in Ryugu samples. The heating experiments of the Orgueil samples are designed to test the effects of removing interlayer water for comparison with the Ryugu samples. This hypothesis is based on the assumption that at least some interlayer water in CI chondrite saponite is terrestrial in origin and that this might explain why both $\Delta'^{17}O$ and $\delta^{18}O$ values for some Ryugu samples tend to be greater than a majority of CI data (this trend is not universal; the Göttingen laboratory obtained $\Delta'^{17}O = 0.78$ for the Alais CI chondrite).

Heating experiments on Orgueil powder were conducted in a tube furnace connected to a turbomolecular pumping station. As shown in Figure 1 and Table 1, results from heating to 250°C and 350°C over 5 hr exhibit mass losses of 7.5%, 13.9%, and 24.9%, with correspondingly increasing $\Delta'^{17}O$ values of 0.331‰ ± 0.010‰, 0.360‰ ± 0.010‰, and 0.452‰ ± 0.011‰, respectively. Similarly, $\delta^{18}O$ increased from a starting value of about 20.0‰ to 23.85‰ ± 0.01‰ with progressive mass loss due to heating.

The source of the oxygen removed by heating was traced using laser-Raman spectra collected from three additional samples of Orgueil exposed to different temperatures, including unheated, heating at 120°C for 2 hr, and heating at 350°C for 5 hr. The heating experiment undertaken at 120°C for 2 hr simulates the preheating procedure using an IR lamp in vacuum prior to fluorination at UCLA (see details in Section 2). The motivation is to verify that surface adsorbed water is indeed largely removed by this procedure. Heating to 250°C and 350°C for 5 hr was used to drive out interlayer water (King et al. 2015). The sample mounts for Raman analyses were carefully prepared without any auxiliary fluid (see details in Section 2). The spectra shown in Figure 2 are the average of between 9 and 13 individual spectra for each sample. The region of the Raman spectra exhibiting stretching modes of water from 3000 to 3800 cm$^{-1}$ (e.g., Shahar & Bassett 2005; Kolesov 2006; de Ligny et al. 2013; Grishina et al. 2021) displays a complex profile of overlapping bands in all three samples. The five bands at 3066, 3194, 3306, 3400, and 3510 cm$^{-1}$ used to fit the spectra are consistent with analogous molecular water features observed in other water-bearing minerals, like those in kimberlite inclusions (e.g., Grishina et al. 2021). The overlapping bands of water include both molecular $H_2O$ and hydroxyl. Previous work on hydrous materials (e.g., Schmidt et al. 1998; Grishina et al. 2021) shows that the O–H stretching mode in hydroxyl ($\sim$3600 cm$^{-1}$) has higher frequency than that in molecular $H_2O$. In our study, due to the overwhelmingly abundant molecular $H_2O$ relative to hydroxyl, we do not resolve an O–H stretch for hydroxyl alone at $\sim$3600 cm$^{-1}$. We interpret the band at 3510 cm$^{-1}$ to be a blend of both molecular $H_2O$ and hydroxyl, whereas the remaining four peaks at 3000–3400 cm$^{-1}$ are mainly stretching modes from molecular $H_2O$ coming from absorbed and interlayer water. Bands at 2800–3000 cm$^{-1}$ correspond to C–H bonds (Bulkin & Krishnan 1971; Romero-Pastor et al. 2011). The apparent loss of the prominent peak at 3194 cm$^{-1}$ in the spectra after heating to 120°C for 2 hr suggests efficient removal of adsorbed molecular water from chips of Orgueil under these conditions.

The water loss associated with various heating conditions can be quantified using the integrated intensities of water bands for the average spectra at 3000–3800 cm$^{-1}$ normalized to the persistent C–H peaks (2800–3000 cm$^{-1}$) for individual spectra. The normalized relative integrated intensities of water decreased from $24.61 \pm 6.31$ ($1\sigma$, $n = 12$) to $15.77 \pm 3.79$ ($1\sigma$, $n = 9$) in our heating experiments. More than 30% of the water present prior to heating was in the form of adsorbed water that is lost at 120°C.

Both $\Delta'^{17}O$ and $\delta^{18}O$ increase with loss of water, though none of the heated Orgueil samples achieve $\Delta'^{17}O$ values as high as that obtained from Ryugu samples. Converting mass loss to oxygen fraction assuming that it is entirely due to water, the oxygen balance equations become

$$\delta^{18}O_{meas} = \Delta x_{H_2O}(\delta^{18}O_{ah} - \delta^{18}O_{H_2O}) + [\delta^{18}O_{ah} + x^0_{H_2O}(\delta^{18}O_{H_2O} - \delta^{18}O_{ah})] \quad (1)$$

and

$$\Delta'^{17}O_{meas} = \Delta x_{H_2O}(\Delta'^{17}O_{ah} - \Delta'^{17}O_{H_2O}) + [\Delta'^{17}O_{ah} + x^0_{H_2O}(\Delta'^{17}O_{H_2O} - \Delta'^{17}O_{ah})], \quad (2)$$
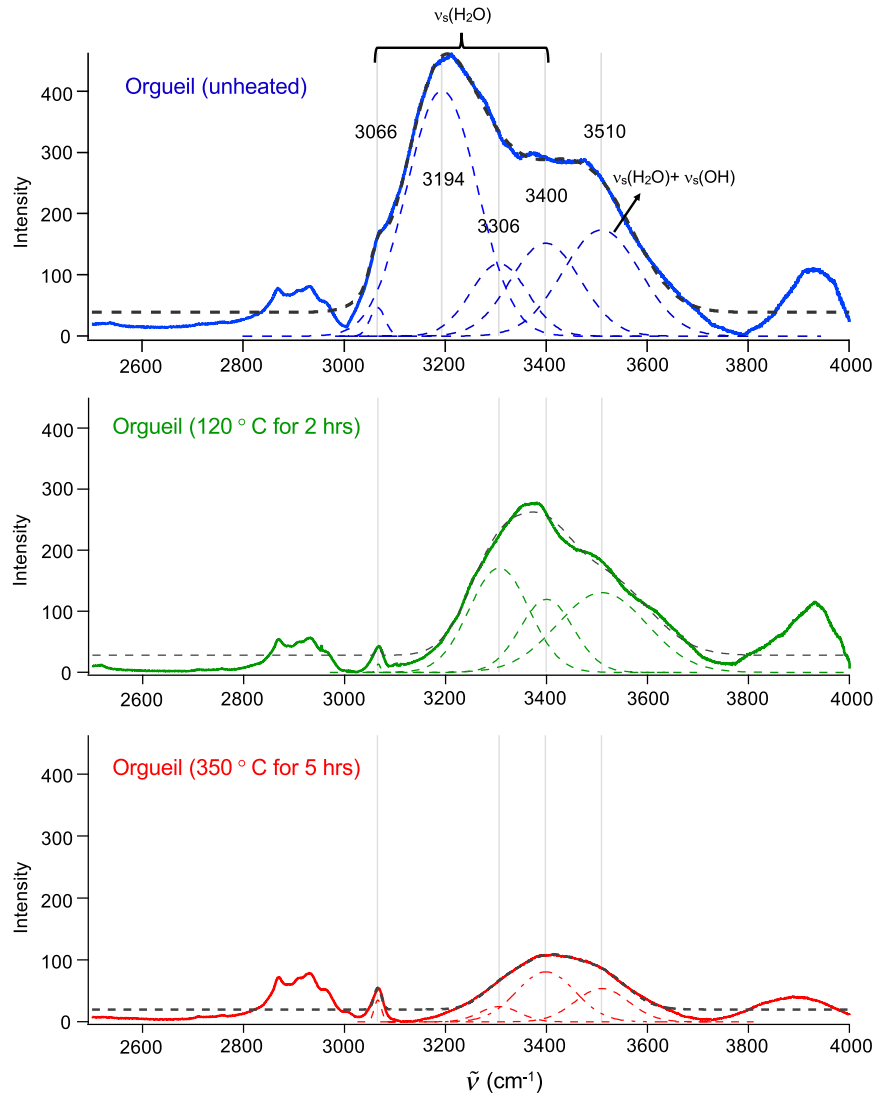
**Figure 2.** Raman spectra for fragments of the Orgueil meteorite heated under vacuum. Conditions include unheated (blue), heating to 120°C for 2 hr under vacuum (green), and vacuum heating at 350°C for 5 hr (red). Thick dashed lines show the fits to the data. Five bands were identified in the stretching region of water at 3000–3800 cm$^{-1}$, shown by the thin dashed lines. Frequencies for the model peaks are labeled and indicated by the vertical gray solid lines. Note the disappearance of the peak at 3194 cm$^{-1}$, indicating the removal of adsorbed molecular water.

where $\Delta x_{H_2O}$ is the oxygen fraction lost as water, $x^0_{H_2O}$ is the oxygen fraction of water prior to heating, and "$H_2O$" and "ah" refer to the interlayer water and the rock-excluding interlayer water, respectively. The use of the prime notation in Equation (2) is an approximation that introduces an error in the fifth decimal digit for values of $\Delta'^{17}O$. Here $\Delta x_{H_2O}$ is calculated from the mass fraction of water lost using

$$\Delta x_{H_2O} = \frac{N_{H_2O} x_{mass}}{N_{H_2O} x_{mass} + N_{ah}(1 - x_{mass})}, \qquad (3)$$

where $N_i$ is the ratio of the number of oxygen atoms per formula unit to molecular weight for the indicated species and $x_{mass}$ is the fraction of mass loss. For example, $H_2O$ has one oxygen atoms per formula unit and a molecular weight of 0.018 kg mol$^{-1}$, yielding $N_{H_2O} = 1/0.018 = 55.56$. Similarly, $N_{ah}$ is estimated to be ~31 assuming that serpentine with the ideal formula $(Mg,Fe)_3Si_2O_5(OH)_4$ and $Mg/(Mg+Fe) \times 100$ (Mg#) of $74-92$ is representative of the rock. Assuming

serpentine with Mg# = 80 as the dominant phase, the mass losses of 7.5%, 13.9%, and 24.9% yield $\Delta x_{H_2O}$ values of 0.13, 0.23, and 0.38, respectively. Equations (1) and (2) show that the slopes derived from plots of oxygen isotopic ratios against $\Delta x_{H_2O}$ values indicate the difference in oxygen isotopic ratios between interlayer water and the remainder of the rock. Regression of the three data points yields $\Delta'^{17}O_{ah} - \Delta'^{17}O_{H_2O} = 0.496\text{‰}$ (Figure 3(a)) and $\delta^{18}O_{ah} - \delta^{18}O_{H_2O} = 15.70\text{‰}$ (Figure 3(b)). The plausible range of Mg# values obtained from chemical analyses yields a narrow range in $\Delta'^{17}O_{ah} - \Delta Op_{H_2O} \Delta'^{17}O_{H_2O}$ values of $0.49\text{‰}-0.50\text{‰}$. With the assumption that terrestrial interlayer water dominates the mass loss during the heating experiments, with $\Delta'^{17}O_{H_2O} = 0\text{‰}$, our results suggest that the pristine samples of the Orgueil meteorite have a $\Delta'^{17}O$ value of 0.496‰. This result is consistent with the hypothesis that CI meteorites exhibit variability in $\Delta'^{17}O$ values, in part due to variable interlayer $H_2O$ of terrestrial origin. Therefore, one expects that some CI

7
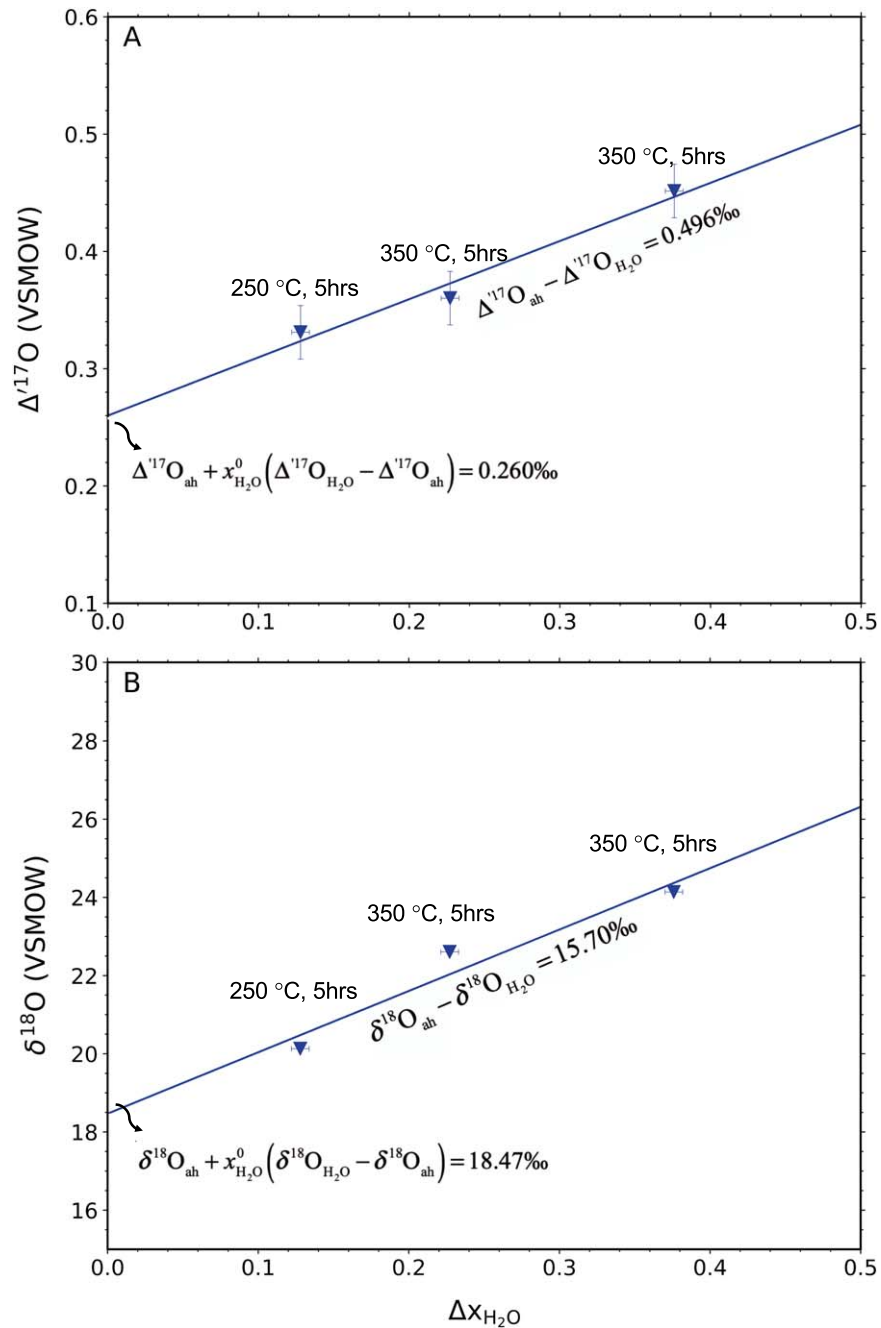
**Figure 3.** Plots of (a) $\Delta'^{17}O$ and (b) $\delta^{18}O$ for the heated Orgueil samples vs. the oxygen fraction lost during heating, $\Delta x_{H_2O}$. The values for fraction of oxygen loss are calculated using Equation (3). The slopes denote the isotopic differences between the interlayer water and remaining rock (see Equations (1) and (2)).

meteorite samples exhibit lower $\Delta'^{17}O$ values compared to the Ryugu samples that have little interlayer $H_2O$, in part due to contamination by terrestrial water. Similar results obtain for $\delta^{18}O$, where the component lost by heating has apparent $\delta^{18}O$ values 15.70‰ lower than the remainder. This value is a convolution of differences in $\delta^{18}O$ and the isotope fractionation effects of removing water. The heated Orgueil samples have $\delta^{18}O$ values reminiscent of samples previously referred to as CY chondrites (King et al. 2019; see Figure 1).

In principle, the intercepts obtained from Equations (1) and (2) can be utilized to estimate the mass fraction of interlayer water in the Orgueil samples prior to heating. However, calculation of $(x_{H_2O}^0)$ is confounded by lack of a priori

information about the isotopic compositions of the interlayer water and phyllosilicates excluding interlayer water.

The comparison of bulk oxygen isotopic ratios between Ryugu samples and CI chondrites suggests that Ryugu samples resemble CI chondrites in their "bulk" oxygen isotope ratios at the milligram scale. Similar to CI chondrites, the heterogeneity in modal mineralogy among samples is a likely explanation for the dispersion in results. In addition, CI chondrites include terrestrial minerals such as sulfates (Airieau et al. 2001, 2005; Gounelle & Zolensky 2001), which may also in part contribute terrestrial oxygen to CI chondrites, driving their oxygen isotope ratios toward terrestrial $\Delta'^{17}O$ values. The presence of these minerals may explain why even our heated Orgueil samples do not have $\Delta'^{17}O$ values as high as the Ryugu samples. The
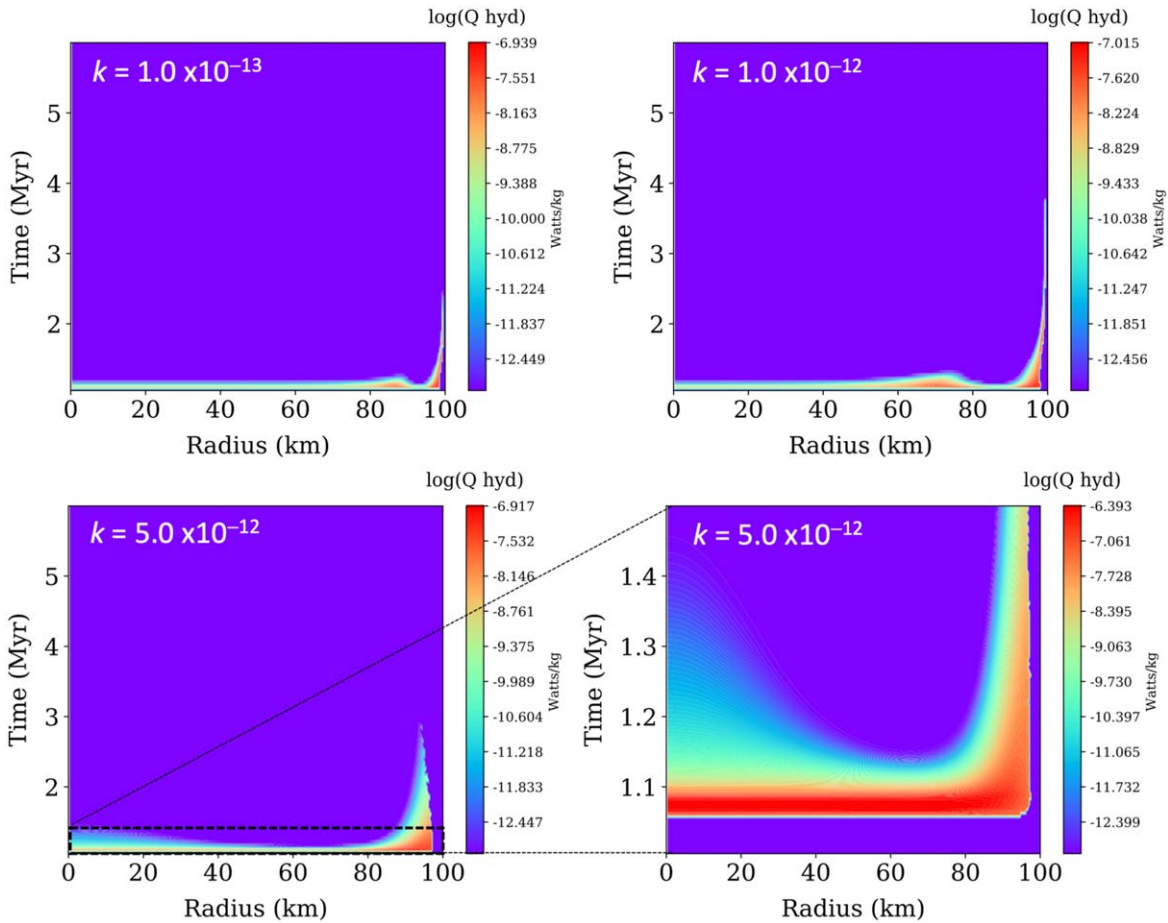
**Figure 4.** Heat of hydration maps for a 100 km planetesimal containing 30% by volume water ice upon instantaneous accretion at 1 Myr post-CAI. Where the heat production (W kg$^{-1}$) is high (warm colors) at a given time (ordinate) and radial position (abscissa), alteration is active in the model. Each panel refers to results for the indicated value for permeability, $k$. Where no heat of hydration is indicated, either hydration has gone to completion or water has been lost owing to hydraulic fracturing (see Section 2). The bottom right panel focuses in on the details of the $k = 5 \times 10^{-12}$ m$^2$ model. The maps show where and when aqueous alteration is predicted to occur in each body.

results of the heating experiments illustrate the tendency of these rocks to acquire exogenous water, adding to heterogeneity among meteorite samples, and possibly a small difference in $\Delta'^{17}O$ between CI chondrites and Ryugu samples.

### 4.2. Constraints on the Ryugu Parent Body

C-type asteroids of all varieties constitute approximately 66% by mass of the asteroid belt, and Brightest Cluster Galaxy (BCG) subclasses, to which Ryugu belongs, constitute ∼40% of the belt by mass (Vernazza et al. 2017). Since Ryugu belongs to a common class of asteroid, and a bias among near-Earth asteroids toward more BCG asteroids relative to the Main Belt is not evidenced (e.g., Marsset et al. 2022), we can consider that Ryugu is a random sample of C-type asteroids sensu lato. This, in turn, implies that this material is relatively common. Because Ryugu is a rubble pile, the size of the parent body in which the retrieved rocks evolved is not known. However, the sampling of CI-like material from Ryugu suggests that aqueous alteration was pervasive in C-type asteroids, rather than highly localized. This conclusion is supported by models for accumulation of rubble piles from larger parent bodies (e.g., 50 km radius). The models indicate that Ryugu should have sampled material from all depths within the parent body, suggesting that Ryugu is representative

of the bulk of the original planetesimal (Sugita et al. 2019), and that this planetesimal was aqueously altered deep within the body.

Based on this premise, thermal modeling can be used to constrain the characteristics of the Ryugu parental planetesimal conducive to producing low-temperature aqueous alteration on a large scale. The heat source in these models is primarily the decay of the short-lived radioisotope $^{26}$Al (e.g., Castillo-Rogez et al. 2009; see Appendix B). We focus our results on the location and timing of the serpentinization reaction that produces Ryugu-like material. Serpentinization depends on the availability of water, which in turn depends on prospects for loss of water due to boiling and escape through fractures, and on circulation due to convection through the permeable host rocks.

The progress of the serpentinization reaction is given by $d\xi_{hyd} = k_{hyd}(1 - \xi_{hyd})dt$, where the rate constant $k_{hyd}$ is obtained from Delescluse & Chamot-Rooke (2008; see Appendix B) and $(1 - \xi_{hyd})$ accounts for the progressive loss of reactants as the reaction proceeds in any one location. Heating due to the exothermic hydration reaction is included using $(d\xi_{hyd}/dt)|\Delta H_{hyd}|$, where $\Delta H_{hyd}$ is the enthalpy of the serpentinization reaction (see Appendix B). Estimates for the temperature of aqueous alteration in Ryugu and for CI chondrites are approximately $50°C \pm 50°C$ (323 K; Bullock
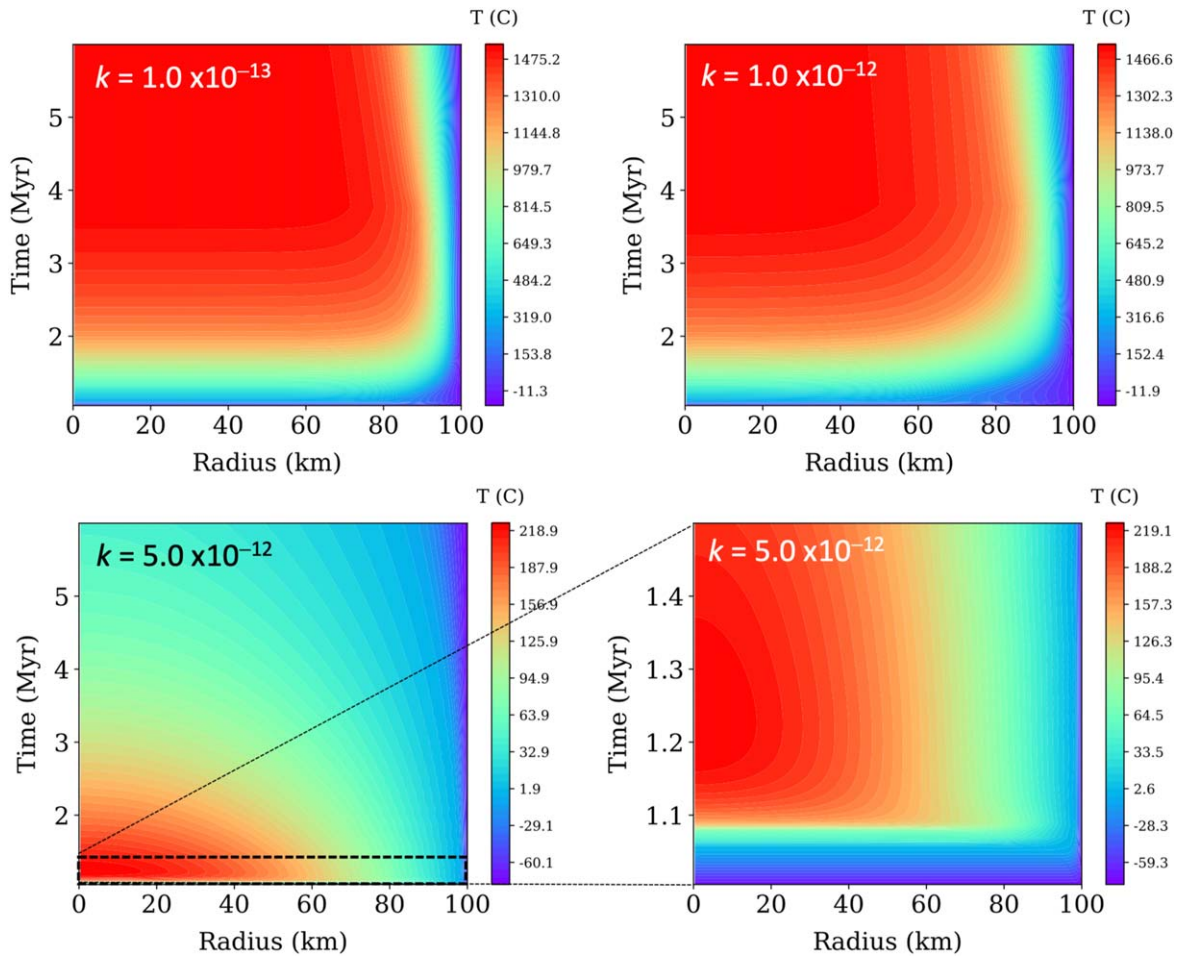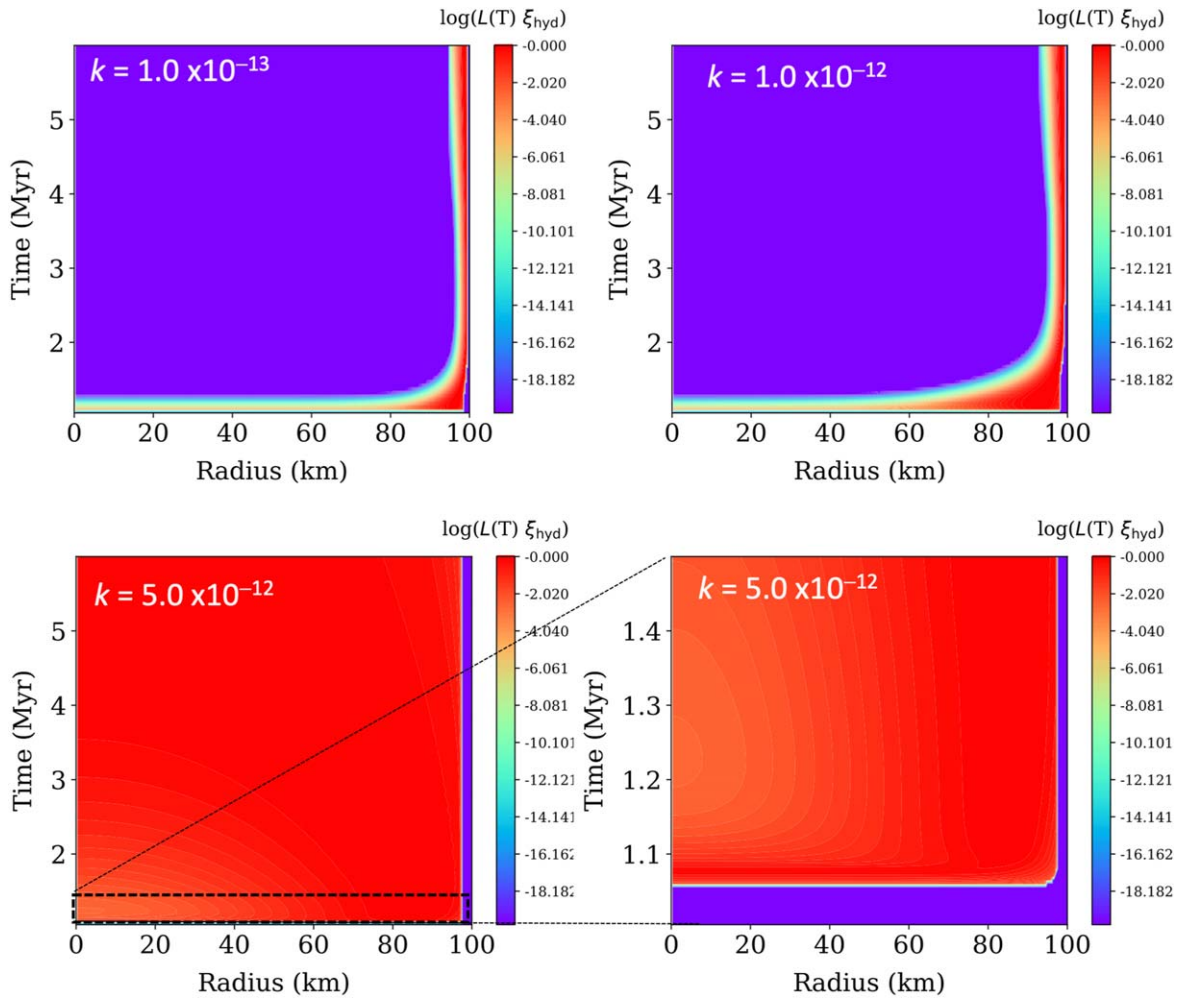
**Figure 5.** Temperatures for the models shown in Figure 4.

et al. 2005; Yokoyama et al. 2023). A good fit to the data is therefore obtained where $\xi_{hyd} \sim 1$ and the model temperature matches the measured temperatures within the uncertainties of the latter. We calculate the likelihood of finding a completely altered rock formed at $323 \pm 50$ K ($50°C \pm 50°C$) using $\mathcal{L}(T) \times \xi_{hyd}$, where $\mathcal{L}(T) = \exp(-0.5(T - 323)^2/50^2)$, as a function of time and radial position in model planetesimals. This formulation of the likelihood function, $\mathcal{L}(T) \times \xi_{hyd}$, assigns a high likelihood of matching the Ryugu alteration conditions for both prograde mineral growth at $50°C \pm 50°C$ and retrograde serpentinization where alteration mineral assemblages may equilibrate to these temperatures during cooling after hydration at higher temperatures (e.g., near $200°C$ but well below dehydration temperatures; Kempf et al. 2022).

Because of the rate of heat transfer through rocks and water, planetesimals larger than approximately 50 km behave similarly in retaining significant portions of the heat released by $^{26}$Al decay. Conversely, the thermal histories of smaller bodies are markedly size dependent owing to the greater radiating surface areas. We take as a fiducial "large" planetesimal a body 100 km in radius (Sugita et al. 2019) containing 30% by volume water ice acquired during instantaneous accretion 1 Myr after "time zero," where time zero is defined as when the ratio of $^{26}$Al relative to the stable isotope $^{27}$Al was $5.2 \times 10^{-5}$, as indicated by calcium–aluminum-rich inclusions (CAIs; e.g., Jacobsen 2008; MacPherson et al. 2010; Larsen et al. 2011). The example ice volume fraction of 30% is comparable to the

value implied by the bulk density of the C-type asteroid 1 Ceres, which appears to be an intact planetesimal. Results are qualitatively similar for ice fractions of 10%–50%. This estimate is also supported by our "$H_2O$ in Murchison" experiment, in which the permeability of Murchison allows for a ~20% water fraction to fill pore spaces (see Appendix C). Aqueous alteration has been dated to <5 Myr post-CAI formation for Ryugu and for other CI chondrites (Endress et al. 1996; Hoppe et al. 2007; Petitat et al. 2011; Fujiya et al. 2013; Visser et al. 2020), and so we focus on early accretion times.

Aqueous alteration occurs within 0.1 Myr of accretion of the bodies in our fiducial models (Figure 4). We find that the prospects for pervasive aqueous alteration at temperatures similar to those evidenced by Ryugu and by CI chondrites depend critically on the permeability ($k$) of the rocks at the time of alteration and the vigor of convection of pore waters. For $k = 1 \times 10^{-13}$ m$^2$, representing a high value for lithified rocks, and two orders of magnitude greater than the values measured for carbonaceous chondrites (Corrigan et al. 1997), the alteration is overprinted by higher temperatures (Figure 5), resulting in restricted zones of preserved, Ryugu-like, low-temperature alteration (within ~10 km of the surface; Figure 6). This is despite active convection that tends to suppress radial temperature gradients. Lower permeabilities yield similarly shallow depths of alteration. Results are similar for an accretion time of 2 Myr. For a 3 Myr accretion time, alteration begins 3.5 Myr after CAI formation, and Ryugu-like

**Figure 6.** Log of likelihood functions for the models shown in Figure 4. Warm colors indicate a high likelihood for finding altered rocks resembling Ryugu samples (maximum = 1).

alteration occurs to depths of ∼20 km. At later accretion times where CI-like alteration occurs much deeper within the bodies, the alteration occurs later than the 5 Myr post-CAI minimum age of the alteration provided by radiometric dating of carbonates. For example, for a 100 km radius body assembled 4 Myr post-CAI, the hydration is predicted to begin at 7 Myr.

However, there is a threshold permeability of $k \sim 5 \times 10^{-12}$ m$^2$ above which convection of the water-rich fluids distributes heat efficiently enough to limit temperatures to ≲230°C throughout the body (Figure 5), resulting in pervasive alteration similar to Ryugu almost everywhere in the body except in the very near surface layers (Figure 6). The low gravitational acceleration for the parent body, combined with similar permeabilities in terrestrial sediments at depths corresponding to pressures similar to those in the parent body (≤30 bar; Ingebritsen & Manning 1999), suggests that the permeabilities used here are easily sustainable against gravitational collapse. These high permeabilities required for this pervasive alteration are several orders of magnitude greater than measured values for carbonaceous chondrites (Corrigan et al. 1997) and resemble those of unconsolidated sand (Forster et al. 2003; Young et al. 2003). Convection of unconsolidated material in planetesimals has been modeled previously (Bland & Travis 2017).

The presence of carbonate-filled fractures (veins) in rocks on asteroid Bennu (Kaplan et al. 2020), rocks thought to be similar

in many respects to those composing Ryugu, makes the hypothesis of high permeabilities due to poor lithification unlikely, at least during the later stages of alteration. If such high permeabilities are considered unrealistic, then the alternative is that aqueous alteration like that in Ryugu occurred in small planetesimals of order a few kilometers that formed early enough to melt water ice. A 5 km radius plantesimal accreted 1 Myr post-CAI would result in pervasive, low-temperature alteration despite being too small for convection (Figure 7). Small bodies may have resulted in part from cycles of accretion and disruption (Wilson et al. 1999). Lack of hydrothermal circulation of fluids in small bodies may explain the preservation of solar-like elemental abundances in these highly altered rocks.

We conclude that the Ryugu rocks formed in a larger (radii >50 km) planetesimal prior to lithification, or in smaller bodies of order a few kilometers in radius if rocks were fully lithified at the time of alteration, as seems most likely. In either case, alteration could have begun in the first million years of the early solar system.

## 5. Conclusions

Our heating experiments reinforce the close correspondence between Ryugu and CI chondrites. Small differences in $\Delta'^{17}$O
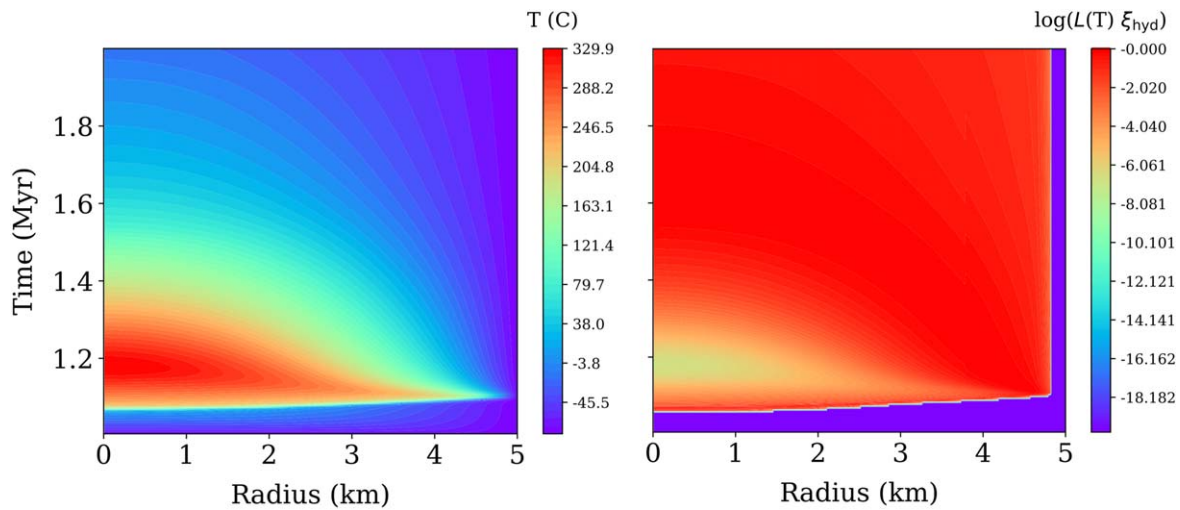
**Figure 7.** Thermal model for a 5 km radius planetesimal accreted with 30% by volume water ice instantaneously at 1 Myr post-CAI. Temperatures as a function of radial distance from the center and time are shown in the left panel, and likelihood for finding low-temperature alteration is shown in the right panel.

between Ryugu samples and CI chondrites are explained at least in part by contamination of the latter by terrestrial water. The discovery that a randomly sampled C-complex asteroid is composed of CI-chondrite-like rock, when combined with thermal models for formation within the first million years of solar system evolution, suggests that the Ryugu parent body, if lithified at the time of alteration, was small (≪50 km radius). If the parent planetesimal was large (>50 km in radius), it was likely composed of high-permeability, poorly lithified sediment rather than consolidated rock.

## Appendix A
## Supplemental Oxygen Isotope Data

Table A1 shows the summary of oxygen data of terrestrial samples to monitor the accuracy of the analyses. Figure A1 demonstrates the temperature of a sample of the Orgueil meteorite being heated up in the laser fluorination chamber at UCLA in order to eliminate surface absorbed water.

**Table A1**
Summary of Oxygen Isotope Data for Terrestrial Samples with $1\sigma$ Errors

| Samples | $\delta^{18}O$ $(1\sigma)$ | $\delta^{17}O$ $(1\sigma)$ | $\Delta^{17}O$ $(1\sigma)$ | $\Delta'^{17}O$ $(1\sigma)$ |
|---|---|---|---|---|
| *Geostandards from UCLA* | | | | |
| Air $O_2$ | $23.785 \pm 0.005$ | $12.126 \pm 0.010$ | $-0.242 \pm 0.010$ | $-0.358 \pm 0.010$ |
| | $23.854 \pm 0.003$ | $12.117 \pm 0.008$ | $-0.287 \pm 0.008$ | $-0.402 \pm 0.008$ |
| Gore Mtn garnet | $5.606 \pm 0.006$ | $2.878 \pm 0.012$ | $-0.037 \pm 0.012$ | $-0.078 \pm 0.012$ |
| SC olivine | $5.270 \pm 0.008$ | $2.679 \pm 0.015$ | $-0.061 \pm 0.016$ | $-0.100 \pm 0.016$ |
| | $5.448 \pm 0.007$ | $2.765 \pm 0.014$ | $-0.068 \pm 0.014$ | $-0.108 \pm 0.014$ |
| *Geostandards from University of Göttingen* | | | | |
| Air $O_2$ | $23.838 \pm 0.160$ | $12.069 \pm 0.080$ | $-0.327 \pm 0.010$ | $-0.442 \pm 0.010$ |
| SC olivine | $5.216 \pm 0.160$ | $2.692 \pm 0.080$ | $-0.020 \pm 0.010$ | $-0.058 \pm 0.010$ |
| | $5.087 \pm 0.160$ | $2.641 \pm 0.080$ | $-0.004 \pm 0.010$ | $-0.042 \pm 0.010$ |
| | $5.237 \pm 0.160$ | $2.707 \pm 0.080$ | $-0.016 \pm 0.010$ | $-0.055 \pm 0.010$ |
| | $5.240 \pm 0.160$ | $2.710 \pm 0.080$ | $-0.015 \pm 0.010$ | $-0.054 \pm 0.010$ |
| | $5.349 \pm 0.160$ | $2.764 \pm 0.080$ | $-0.017 \pm 0.010$ | $-0.056 \pm 0.010$ |
| | $4.867 \pm 0.160$ | $2.521 \pm 0.080$ | $-0.010 \pm 0.010$ | $-0.046 \pm 0.010$ |
| | $5.225 \pm 0.160$ | $2.684 \pm 0.080$ | $-0.033 \pm 0.010$ | $-0.071 \pm 0.010$ |
| | $5.020 \pm 0.160$ | $2.578 \pm 0.080$ | $-0.032 \pm 0.010$ | $-0.069 \pm 0.010$ |
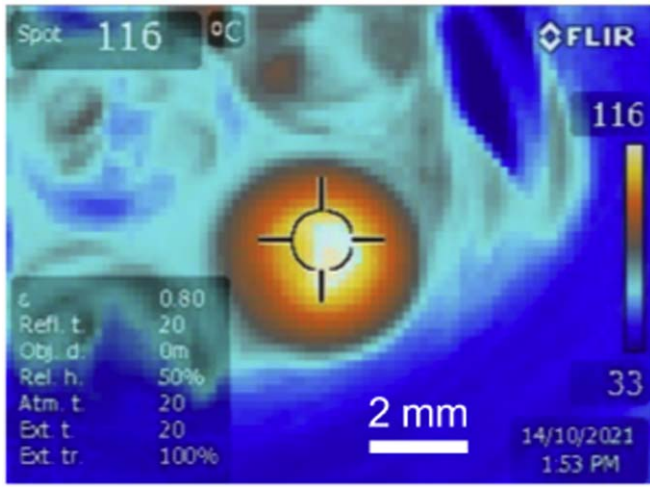


**Figure A1.** Infrared image showing temperature of a sample of the Orgueil meteorite being heated up to 116°C in the laser fluorination chamber at UCLA. Samples are heated for ∼2 hr at these temperatures to eliminate surface absorbed water prior to fluorination.

## Appendix B
## Thermal Modeling

Thermal models were computed using methods described previously in Zhou et al. (2013) and Tang & Young (2021). Briefly, we solved the equation for conductive heat transfer in a sphere at each radial position $r_i$ with internal heat production $Q$:

$$\frac{\partial T}{\partial t} = \kappa \left( \frac{\partial^2 T}{\partial r^2} + \frac{2}{r}\frac{\partial T}{\partial r} \right) + (1 - \phi)\frac{Q}{c}, \quad (B1)$$

where $\kappa$ is the thermal diffusivity, or effective thermal diffusivity; $c$ is the effective heat capacity; $\phi$ is the volumetric fraction of the body initially composed of ice (water ice in this case); and $T$ is temperature. Equation (B1) is solved using explicit finite difference with a surface boundary condition defined by a balance between conductive and radiative heat fluxes at the surface:

$$K_S \left( \frac{\partial T}{\partial r} \right)_S - \sigma(T_S^4 - T_b^4) = 0, \quad (B2)$$

where $T_S$ and $T_b$ are the surface and ambient background temperatures, respectively, $K_S$ is the thermal conductivity at the surface, and the partial derivative is evaluated at the surface. The details of solving Equations (B1) and (B2) are described by Tang & Young (2021). Results are shown for a formation distance from the Sun of 2 au and assume present-day solar parameters. The details of the formation distance and resulting surface temperature are not crucial for the results shown.

We included the thermal effects of water phase changes, including the irreversible amorphous-to-crystalline-ice transition and the reversible ice−liquid, ice−vapor, and liquid −vapor transitions. Three reaction progress variables were used to track the phase transitions:

$$\xi_{H_2O\ melting} = \sum_i \frac{c_{H_2O_i}(T_i - 270)}{\Delta H_{H_2O\ melting}}$$

$$\xi_{H_2O\ xstln} = \frac{c_{H_2O_i}(130 - T_i)}{\Delta H_{xstln}}$$

$$\xi_{sub} = \frac{c_{H_2O_i}(T_i - 180)}{\Delta H_{sub}}, \quad (B3)$$

where subscripts melting, xstln, and sub refer to melting, crystallization, and sublimation, respectively. Enthalpies of phase transitions are accommodated at each location and each time step through the specific heat in Equation (B1). Upon

heating, the specific heat is calculated using

$$
\begin{aligned}
c_i = 1050 &+ \left(\frac{\Delta H_{\text{sil melt}}}{\Delta T_{\text{sil melt}}}\right) \int_{\xi_{\text{sil melt,i}}=0}^{\xi_{\text{sil melt,i}}=1} \\
&\times (1 - \xi_{\text{sil melt},i})\, \delta(\xi_{\text{sil melt}} - \xi_{\text{sil melt},i}) d\xi_{\text{sil melt}} \\
&+ \left(\frac{\Delta H_{\text{xstln}}}{\Delta T_{\text{xstln}}}\right)\left(\frac{\phi}{1-\phi}\right)\frac{\rho_{\text{ice}}}{\rho_{\text{rock}}} \int_{\xi_{\text{xstln}}=0}^{\xi_{\text{xstln}}=1} \\
&\times (1 - \xi_{\text{xstln},i})\delta(\xi_{\text{xstln}} - \xi_{\text{xstln},i}) d\xi_{\text{xstln}} \\
&+ \left(\frac{\Delta H_{\text{sub}}}{\Delta T_{\text{sub}}}\right)\left(\frac{\phi}{1-\phi}\right)\frac{\rho_{\text{ice}}}{\rho_{\text{rock}}} \int_{\xi_{\text{sub,i}}=0}^{\xi_{\text{sub,i}}=1} \\
&\times (1 - \xi_{\text{sub},i})\, \delta(\xi_{\text{sub}} - \xi_{\text{sub},i}) d\xi_{\text{sub}} \\
&+ \left(\frac{\Delta H_{\text{H}_2\text{O melt}}}{\Delta T_{\text{H}_2\text{O melt}}}\right)\left(\frac{\phi}{1-\phi}\right)\frac{\rho_{\text{H}_2\text{O}}}{\rho_{\text{rock}}} \int_{\xi_{\text{H}_2\text{O melt,i}}=0}^{\xi_{\text{H}_2\text{O melt,i}}=1} \\
&\times (1 - \xi_{\text{H}_2\text{O melt},i})\, \delta(\xi_{\text{H}_2\text{O melt}} - \xi_{\text{H}_2\text{O melt},i}) d\xi_{\text{H}_2\text{O melt}},
\end{aligned} \quad \text{(B4)}
$$

where 1050 is the specific heat for rock (J (kg K)$^{-1}$); the enthalpies of transition, temperature intervals of transition, and densities are represented by the standard symbols; and $\rho\text{H}_2\text{O}$ is the density of the reactant water phase. Upon cooling, we use

$$
\begin{aligned}
c_i = 1050 &- \left(\frac{\Delta H_{\text{sil melt}}}{\Delta T_{\text{sil melt}}}\right)\int_{\xi_{\text{sil melt,i}}=0}^{\xi_{\text{sil melt,i}}=1} \\
&\times \xi_{\text{sil melt},i}\, \delta(\xi_{\text{sil melt}} - \xi_{\text{sil melt},i}) d\xi_{\text{sil melt}} \\
&- \left(\frac{\Delta H_{\text{H}_2\text{O melt}}}{\Delta T_{\text{H}_2\text{O melt}}}\right)\left(\frac{\phi}{1-\phi}\right)\frac{\rho_{\text{H}_2\text{O}}}{\rho_{\text{rock}}} \\
&\times \int_{\xi_{\text{H}_2\text{O melt,i}}=0}^{\xi_{\text{H}_2\text{O melt,i}}=1} \xi_{\text{H}_2\text{O melt},i}\, \delta(\xi_{\text{H}_2\text{O melt}} - \xi_{\text{H}_2\text{O melt},i}) d\xi_{\text{H}_2\text{O melt}}.
\end{aligned} \quad \text{(B5)}
$$

The integrals of the form

$$
\int_{\xi_i=0}^{\xi_i=1} f(\xi_i)\, \delta(\xi - \xi_i) d\xi = \begin{cases} f(\xi_i) & \text{if } 0 < \xi_i < 1 \\ 0 & \text{for all other values for } \xi_i \end{cases}
$$

in Equations (B4) and (B5) are Dirac measures of reaction progress at each location $i$, and $\delta$ are Dirac delta functions. Values for $f(\xi_i)$ evaluate to $1 - \xi_i$ or $\xi_i$ when $0 < \xi_i < 1$ and 0 for all other values of $\xi_i$. Values for the various parameters required in Equations (B1)−(B5) are given in Table 4 of Zhou et al. (2013).

The reaction progress for serpentinization (hydration) is obtained numerically using

$$
\frac{d\xi_{\text{hyd}}}{dt} = k_{\text{hyd}}(1 - \xi_{\text{hyd}}), \quad \text{(B6)}
$$

where

$$
k_{\text{hyd}} = a_h \exp(-b_h(T - c_h)^2)\xi_{\text{H}_2\text{O melting}} \quad \text{(B7)}
$$

and $a_h = 8 \times 10^{-12}\ s^{-1}$, $b_h = 2.5 \times 10^{-4}\ K^{-2}$, and $c_h = 400$ K. These constants are from Delescluse & Chamot-Rooke (2008), with the exception that we revised $c_h$ downward from their original value of 540 K. With this adjustment the peak in the rate constant occurs at 400 K (120°C). The reaction progress variable for melting of water ice, $\xi_{\text{H}_2\text{O melting}}$, is generally 0 or 1 and ensures that the hydration reaction only occurs where liquid water is present.

We used a value of $\Delta H_{\text{hyd}} = -305.64$ kJ kg$^{-1}$ (of reactant rock) and incorporated this as an additional source of heat production $Q$ in Equation (B1), where $Q = Q_{\text{radioisotopes}} + Q_{\text{hyd}}$ and $Q_{\text{hyd}} = (d\xi_{\text{hyd}}/dt)|\Delta H_{\text{hyd}}|$.

Dehydration of serpentinized rock, where $\xi_{\text{hyd}} > 0$, is included in the numerical solutions using the rate equation

$$
\frac{d\xi_{\text{hyd}}}{dt} = -k_{\text{dehyd}}, \quad \text{(B8)}
$$

where the temperature-dependent rate constant $k_{\text{dehyd}} = 1 \times 10^{33} \exp(-5.98 \times 10^5/(RT))$ s$^{-1}$ is derived from experimental data (Llana-Fúvenz et al. 2007), and $R$ is the gas constant. Dehydration begins in earnest at ∼620 K (360°C) with this rate constant.

We included approximations to the azimuthally averaged thermal effects of convection of water through the porous rock medium by multiplying the thermal diffusivity by a Nusselt number, Nu, to derive an effective diffusivity Nu$\kappa$. We evaluated Nu using the prescription for the critical Rayleigh number for convection (Ra$_c$) by Young et al. (2003) and the scaling between Nu and Ra given by Grimm & Mcsween (1989), where Nu $= 1.6(\text{Ra}/\text{Ra}_c)^{0.6}$ and Ra is the Rayleigh number. The critical value for Ra of 184 is greater than in many other circumstances owing to the restrictions on flow imposed by finite permeabilities. We evaluated the criterion for convective flow at each time step using (Young et al. 2003)

$$
\text{Ra} = \frac{\alpha\beta\gamma a^4}{K\kappa} > 183.91, \quad \text{(B9)}
$$

where $\alpha = 2.1 \times 10^{-4}$ K$^{-1}$ is the isobaric thermal expansivity of water, $\beta = Q/(3\kappa c)$ is the thermal constant, $\gamma = (4/3)\pi\rho G$ is the gravitational constant, $\rho \sim 2400$ kg m$^{-3}$ is the bulk density of the body, $K = \mu/(\rho_f k)$, $\mu = 8.54 \times 10^{-4}$ Pa s is the fluid viscosity, $k$ is the permeability, and $\rho_f = 995$ kg m$^{-3}$ is the fluid density.

The availability of reactant liquid water where convection does not obtain was included in our calculation by considering the effects of boiling as temperatures increased. The pressures in our models are all below that for the critical point for H$_2$O of 22 MPa. Therefore, pores filled with water produced by melting of ice consist of both liquid and vapor. Where the vapor pressure of water is high, the possibility of fracturing of the rock exists, according to the criterion

$$
P_v - P_c > \tau, \quad \text{(B10)}
$$

where $P_v$ is the vapor pressure of water, $P_c = (2/3)\pi\rho^2 G(a^2 - r^2)$ is the confining pressure due to gravity for rock density $\rho$ at radial position $r$ in a body of radius $a$, and $\tau$ is the tensil strength of the rock. Where the criterion in Equation (B10) obtains and there is no convection, the continuous loss of vapor drains the voids of liquid water in our calculations, which we model as an instantaneous process here, thus preventing further hydration reactions from occurring. We used a value of 2 MPa for $\tau$ based on measured values for carbonaceous chondrites (Slyuta 2017) and a standard Antoine equation for the vapor pressure of H$_2$O to evaluate Equation (B10).

## Appendix C
## H$_2$O in Murchison Experiment

Experiments on the behavior of H$_2$O in the Murchison meteorite were performed with the aim of assessing the permeability of chondrites subjected to aqueous alteration. Murchison was chosen

based on availability and is only a rough analog for the precursors to Ryugu samples. The results are relevant to the choice of the range in permeabilities in our calculations. In this experiment, a piece of $\sim 0.273$ g Murchison was immersed in distilled water for 45 hr at room temperature. The radius of 0.35 cm for the roughly spheroidal Murchison sample corresponds to a volume of 0.18 cm$^3$. The sample bubbled in the first hour of the experiment. The sample was then air-dried briefly until water was invisible at the surface. The sample and absorbed water were then weighed, yielding a combined mass of 0.286 g. The sample was then placed in a drying oven at 60°C for 24 hr to remove the imbibed water, resulting in a mass of 0.261 g after drying. The total moisture removed from the Murchison sample was 0.025 g, which included intrinsic moisture in the sample prior to the experiment and exogenous water introduced during immersion.

We estimate the mass and volume fractions of imbibed water relative to the rock using

$$\frac{\text{mass}_{\text{water}}}{\text{mass}_{\text{rock}}} = \frac{0.025}{0.261} = 0.096 \tag{C1}$$

and

$$\frac{\text{volume}_{\text{water}}}{\text{volume}_{\text{rock}}} = \frac{\text{mass}_{\text{water}}}{\text{mass}_{\text{rock}}} \times \frac{\rho_{\text{rock}}}{\rho_{\text{water}}} = 0.096 \times \frac{2.5}{1} = 0.241, \tag{C2}$$

where the density of the rocky fraction of Murchison ($\rho_{\text{rock}}$) is assumed to be 2.5 g cm$^{-3}$. The volume fraction of water relative to the total volume of the sample therefore is 0.241/(0.241 + 1) = 19.4%. The ingress of this fraction of water, which is only slightly lower than the estimated porosity of CM chondrites of 20–25 vol% (Consolmagno et al. 2008), implies that the Murchison sample is not only porous but also highly permeable. The result allows for the possibility that the Ryugu protoliths were also highly permeable.

## ORCID iDs

Haolan Tang ⓘ https://orcid.org/0000-0002-9293-3662
Edward D. Young ⓘ https://orcid.org/0000-0002-1299-0801
Sachiko Amari ⓘ https://orcid.org/0000-0003-4899-0974
Audrey Bouvier ⓘ https://orcid.org/0000-0002-8303-3419
Richard W. Carlson ⓘ https://orcid.org/0000-0001-7195-2074
Marc Chaussidon ⓘ https://orcid.org/0000-0001-8475-0690
Wataru Fujiya ⓘ https://orcid.org/0000-0003-2578-5521
Ryota Fukai ⓘ https://orcid.org/0000-0002-1477-829X
Hiroshi Hidaka ⓘ https://orcid.org/0000-0002-4067-7679
Trevor R. Ireland ⓘ https://orcid.org/0000-0001-7617-3889
Larry Nittler ⓘ https://orcid.org/0000-0002-5292-6089
Changkun Park ⓘ https://orcid.org/0000-0002-1206-6803
Richard J. Walker ⓘ https://orcid.org/0000-0003-0348-2407
Tetsuya Yokoyama ⓘ https://orcid.org/0000-0003-2247-7232
Shigekazu Yoneda ⓘ https://orcid.org/0000-0003-2306-4261
Masanao Abe ⓘ https://orcid.org/0000-0003-4780-800X
Hisayoshi Yurimoto ⓘ https://orcid.org/0000-0003-0702-0533

## References

Airieau, S., Farquhar, J., Jackson, T., et al. 2001, LPSC, 32, 1744
Airieau, S., Farquhar, J., Thiemens, M., et al. 2005, GeCoA, 69, 4167
Bancroft, G. M., Nesbitt, H. W., Henderson, G. S., et al. 2018, JNCS, 484, 72
Bland, P. A., & Travis, B. J. 2017, SciA, 3, e1602514
Brearley, A. J. 2006, in Meteorites and the Early Solar System II, ed. D. S. Lauretta & H. Y. McSween (Tucson, AZ: Univ. Arizona Press), 587
Bulkin, B. J., & Krishnan, K. 1971, JAChS, 93, 5998
Bullock, E., Gounelle, M., Lauretta, D., Grady, M., & Russell, S. 2005, GeCoA, 69, 2687
Castillo-Rogez, J., Johnson, T. V., Lee, M. H., et al. 2009, Icar, 204, 658
Clayton, R. N., & Mayeda, T. K. 1999, GeCoA, 63, 2089
Consolmagno, G., Britt, D., & Macke, R. 2008, ChEG, 68, 1
Corrigan, C. M., Zolensky, M. E., Dahl, J., et al. 1997, M&PS, 32, 509
Dauphas, N., & Pourmand, A. 2015, GeCoA, 163, 234
de Ligny, D., Guillaud, E., Gailhanou, H., & Blanc, P. 2013, PrEPS, 7, 203
Delescluse, M., & Chamot-Rooke, N. 2008, E&PSL, 276, 140
Endress, M., Zinner, E., & Bischoff, A. 1996, Natur, 379, 701
Forster, S., Bobertz, B., & Bohling, B. 2003, AqGeo, 9, 171
Fujiya, W., Sugiura, N., Sano, Y., & Hiyagon, H. 2013, E&PSL, 362, 130
Gounelle, M., & Zolensky, M. E. 2001, M&PS, 36, 1321
Greenwood, R. C., Franchi, I. A., Findlay, R., et al. 2023, NatAs, 7, 29
Grimm, R. E., & Mcsween, H. Y. 1989, Icar, 82, 244
Grishina, S., Goryainov, S., Oreshonkov, A., & Karmanov, N. 2021, JRSp, 53, 497
Hoppe, P., MacDougall, D., & Lugmair, G. W. 2007, M&PS, 42, 1309
Ingebritsen, S., & Manning, C. E. 1999, Geo, 27, 1107
Jacobsen, B., zhu Yin, Q., & Moynier, F. 2008, E&PSL, 272, 353
Kaplan, H. H., Lauretta, D. S., Simon, A. A., et al. 2020, Sci, 370, eabc3557
Kempf, E. D., Hermann, J., & Connolly, J. A. D. 2022, SwJG, 115, 14
King, A., Bates, H., Krietsch, D., et al. 2019, ChEG, 79, 125531
King, A. J., Solomon, J. R., Schofield, P. F., & Russell, S. S. 2015, EP&S, 67, 198
Kolesov, B. 2006, AmMin, 91, 1355
Larsen, K. K., TRINqUIER, A., Paton, C., et al. 2011, ApJL, 735, L37
Liu, M.-C., McCain, K. A., Matsuda, N., et al. 2022, NatAs, 6, 1172
Llana-Fvönez, S., Brodie, K. H., Rutter, E. H., & Arkwright, J. C. 2007, JMetG, 25, 423
Lodders, K. 2021, SSRv, 217, 44
MacPherson, G. J., Bullock, E. S., Janney, P. E., et al. 2010, ApJL, 711, L117
Marsset, M., DeMeo, F. E., Burt, B., et al. 2022, AJ, 163, 165
McCain, K. A., Matsuda, N., Liu, M.-C., et al. 2023, NatAs, 7, 309
Miller, M. F. 2002, GeCoA, 66, 1881
Morota, T., Sugita, S., Cho, Y., et al. 2020, Sci, 368, 654
Nakashima, D., Nakamura, T., Zhang, M., et al. 2023, NatCo, 14, 532
Pack, A. 2021, RvMG, 86, 217
Pack, A., & Herwartz, D. 2014, E&PSL, 390, 138
Petitat, M., Marrocchi, Y., McKeegan, K. D., et al. 2011, M&PS, 46, 275
Romero-Pastor, J., Cardell, C., Yebra-Rodriguez, A., Manzano, E., & Navas, N. 2011, JRSp, 42, 2137
Rumble, D., Miller, M., Franchi, I., & Greenwood, R. 2007, GeCoA, 71, 3592
Schmidt, B., Holtz, F., & Bény, J.-M. 1998, JNCS, 240, 91
Shahar, A., Bassett, W. A., Mao, H.-K., Chou, I.-M., & Mao, W. 2005, AmMin, 90, 1835
Sharp, Z. D. 1990, GeCoA, 54, 1353
Slyuta, E. N. 2017, SoSyR, 51, 64
Sugita, S., Honda, R., Morota, T., et al. 2019, Sci, 364, eaaw0
Tachibana, S., Abe, M., Arawaka, M., et al. 2014, GeocJ, 48, 571
Tachibana, S., Sawada, H., Okazaki, R., et al. 2022, Sci, 375, 1011
Tanaka, R., & Nakamura, E. 2013, RCMS, 27, 285
Tang, H., & Young, E. D. 2021, Eleme, 17, 401
Tomeoka, K., & Buseck, P. R. 1988, GeCoA, 52, 1627
Vacher, L. G., Piani, L., Rigaudier, T., et al. 2020, GeCoA, 281, 53
Vernazza, P., Castillo-Rogez, J., Beck, P., et al. 2017, AJ, 153, 72
Visser, R., John, T., Whitehouse, M. J., Patzek, M., & Bischoff, A. 2020, E&PSL, 547, 116440
Wasson, J. T., & Kallemeyn, G. W. 1988, RSPTA, 325, 535
Wilson, L., Keil, K., Browning, L. B., Krot, A. N., & Bourcier, W. 1999, M&PS, 34, 541
Yokoyama, T., Nagashima, K., Nakai, I., et al. 2023, Sci, 379, abn7850
Young, E., Yeung, L., & Kohl, I. 2014, GeCoA, 135, 102
Young, E. D., Coutts, D. W., & Kapitan, D. 1998, GeCoA, 62, 3161
Young, E. D., Galy, A., & Nagahara, H. 2002, GeCoA, 66, 1095
Young, E. D., Kohl, I. E., Warren, P. H., et al. 2016, Sci, 351, 493
Young, E. D., Zhang, K. K., & Schubert, G. 2003, E&PSL, 213, 249
Zhou, Q., Yin, Q.-Z., Young, E., et al. 2013, GeCoA, 110, 152